# Journal Pre-proof


Hierarchical molybdenum phosphide coupled with carbon as a whole pH-range electrocatalyst for hydrogen evolution reaction

Riyue Ge, Juanjuan Huo, Ting Liao, Yang Liu, Mingyuan Zhu, Ying Li, Jiujun Zhang, Wenxian Li

PII: S0926-3373(19)30943-9

DOI: https://doi.org/10.1016/j.apcatb.2019.118196

Reference: APCATB 118196

To appear in: *Applied Catalysis B: Environmental*

Received Date: 2 July 2019

Revised Date: 11 September 2019

Accepted Date: 13 September 2019

Please cite this article as: Ge R, Huo J, Liao T, Liu Y, Zhu M, Li Y, Zhang J, Li W, Hierarchical molybdenum phosphide coupled with carbon as a whole pH-range electrocatalyst for hydrogen evolution reaction, *Applied Catalysis B: Environmental* (2019), doi: https://doi.org/10.1016/j.apcatb.2019.118196

# Hierarchical molybdenum phosphide coupled with carbon as a whole pH-range electrocatalyst for hydrogen evolution reaction

Riyue Ge[a], Juanjuan Huo[b], Ting Liao[*,c], Yang Liu[d], Mingyuan Zhu[a], Ying Li[*,a,d], Jiujun Zhang[d], and Wenxian Li[*,a,d]

[a]School of Materials Science and Engineering, Shanghai University, Shanghai 200444, China

[b]School of Environmental and Chemical Engineering, Shanghai University, Shanghai 200444, China

[c]School of Chemistry, Physics and Mechanical Engineering, Queensland University of Technology, Brisbane QLD 4000, Australia

[d]Institute for Sustainable Energy, Shanghai University, Shanghai 200444, China

**Corresponding authors**

[*]E−mail address: shuliwx@t.shu.edu.cn; liying62@shu.edu.cn; t3.liao@qut.edu.au.

Graphical abstract

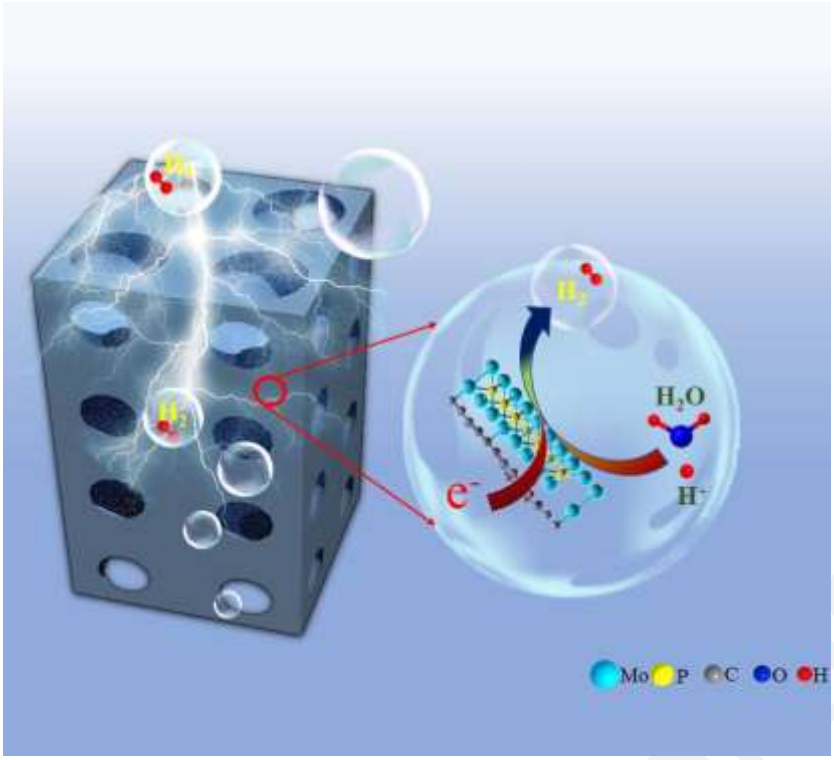


Well−crystallized molybdenum phosphide nanoparticles anchored in three−dimensional N, P−codoped graphite carbon nanosheets (3D MoP/NPG) show excellent catalytic activity and stability under a wide pH range toward HER.

Highlights

- Hierarchically structural electrocatalyst contained of well-crystallized MoP nanoparticles and heteroatoms-doped graphite carbon nanosheets was fabricated.
- The synergetic interaction between heteroatoms-codoped carbon sheets and MoP nanosheets can optimize H adsorption/desorption to enhance catalytic activity.
- Porous heteroatoms-doped carbon architecture as substrate can facilitate charge transfer and mass transport.
- The optimized catalyst possesses significantly improved electrocatalytic activity and durability for HER in a wide pH range toward hydrogen evolution reaction.

**ABSTRACT**

In the effort to develope more effective electrocataysts for water electrolysis hydrogen generation through hydrogen evolution reaction (HER), the well-crystallized molybdenum phosphide nanoparticles dispersed in three−dimensional N,P−codoped graphite carbon nanosheets (3D MoP/NPG) is synthesized in this work using a $SiO_2$-template-assisted strategy. Instrument characterization shows that the catalyst has a large specific surface area, high electrical conductivity, and the coupled interfaces & synergistic effect between MoP and carbon sheets toward electrocatalytic HER. Experimental results reveal that MoP/NPG possesses remarkable catalytic HER activity and stability in a wide pH range. Density functional theory (DFT) calculations reveal that the coupled interaction between MoP and carbon sheet interfaces can induce an optimal free energy of hydrogen adsorption on the catalyst surface. Both the theoretical calculations and experimental results demonstrate that the hierarchical structure with synergistic interaction between MoP and carbon sheets can facilitate charge transfer kinetics to enhance HER performance.

**KEYWORDS:** Electrocatalysts; Molybdenum phosphide; Coupled interaction; Hierarchical structure; Hydrogen evolution reaction

## 1. Introduction

In recent years, exploring renewable and environmentally−friendly energy resources such as solar and wind energy has become entensive due to the fast consumption and depletion of fossil fuels and their associated environment issues.[1−3] With increasing the solar- and wind-electricity stations wildwide, how to store the produced unstable electricity energy has been becoming an urgent research topic in the further development and practical applications of such energy sources.[4] With respect to this, using such unstable electricity energies to electrochemically split

water (electrolysis) to produce hydrogen ($H_2$) to realize energy storage has been considered one of the sustainable solutions.[5−7] In an operating water electrolysis cells, $H_2$ is produced at cathode (negative electrode) through hydrogen evolution reaction (HER), and $O_2$ is generated at anode (positive electrode) through oxygen evolution reaction (OER). Both of these two reactions need electrocatalysts to speed up to reducing electrode overpotentials and increasing energy efficiency for practical hydrogen production.[8-15] The most practical electrocatalysts used for $H_2$ generation at cathode are those noble metals (Pt, Ir, Ru, etc.)−based materials, which are high-cost.[16-18] To reduce the cost, some non-noble metals-based catalysts such as MoP,[19] $MoS_2$,[20] $Mo_xC$,[21,22] MoN,[23] and the other transition metal-based ones[24] have also been explored for catalyzing HER. Normally, the key performance parameters for highly efficient HER electrocatalysts should have high density of active sites, high conductivity, stable structure, and optimal hydrogen adsorption/desorption energy.[25] To achieve these properties of non-noble metals-based catalysts, great effort has been made in recent decade.[26]

Among the explored HER electrocatalysts, the materials with hierarchical porous structure have been found to have ability facilitating the mass transport and optimizing the liquid−to−gas conversion synergistically due to their favorite structures/morphologies, compositions and lage surface areas.[27-29] In synthesis of these catalysts, the templated−assisted methods are widely used to fabricate porous structures through outside or inside space confined growth using removable templates,[27, 30] such as $SiO_2$[31] and polystyrene spheres (PS).[32,33] Three dimensional hollow architecture of graphene,[31] metal particle,[34] and transition metal sulfides[30] have been introduced to impede the agglomeration for increasing the specific surface area. For example, Deng *et al.*[27] synthesized a uniform mesoporous $MoS_2$ foam through a templated-assisted method and the catalyst exhibited both high electrocatalytic activity and durability toward HER due to the large surface area and stable structure. Guan *et al.*[35] synthesized single-holed cobalt/N-doped carbon hollow hybrids with large surface area and stable hollow structure via a carbonization process of polystyrene (PS) spheres, leading to outstanding electrocatalytic

activity and durability toward oxygen reduction reaction (ORR). Normally, the electronic structure and adsorption energy can be modulated by heteroatom doping effect. N, and/or P elements have been employed to dope carbon architectures through activating heteroatom(s)-neighboring carbon atoms to alter the adsorption energy, as confirmed by both experimental results and DFT calculations.[36-39] A synergetic role of the doped heteroatom in carbon lattice and the encapsulated transition metal nanoparticles can stimulate an enhanced intrinsic electrocatlytic activity of the carbon-based materials. Bao *et al.*[40] demonstrated that N-doped graphene encapsulating CoNi nanoparticles could increase the structural stability and corrosion resistance, and optimize the electronic configuration, leading to high activity and long−term stability for HER. Zhang et al.[41] synthesized N and P-codoped 3D porous graphitic carbon hybrid via a pyrolysis method using melamine-phytic acid supermolecular aggregate and graphene oxide as precursors. The obtained hybrid exhibited both high activity and durability toward both ORR and HER due to the large surface area, high conductivity and synergistic effect of N, P codoping.

Among different types of HER electrocatalysts explored, transition−metal phosphides,[42-45] such as MoP, have attracted extensive attentions as effective ones[46-49] for their natural abundance, low−cost, and stable catalytic performance with possibility to replace noble metal catalysts.[50] As reported,[51-54] amorphous structure of MoP nanoparticle could exhibit highly catalytic performance toward HER, resulted from its large specific surface area with a lot of active sites. However, the well−crystallized MoP suffered low content of active sites becasue of the inevitable agglomeration under high phase−forming temperature.[55] Many strategies have been employed to decrease the size of nanoparticles and/or regulate the nanostructures for further enhancement of the catalytic activity and stability of MoP−based catalysts.[56-58] Another strategy is to introduce a conductive support including graphene,[59] carbon nanotubes[60] or other materials[61] to couple with the active sites for enhancing catalytic performance. With respect to this, highly dispersed MoP nanoparticles embedded in N-doped porous carbon nanofibers were

demonstrated as HER catalysts with high catalytic performance.[52] Although many novel catalysts have been developed, they are still lack of competitive catalytic performance compared with noble metal-based catalytic materials and most of the catalytic performance were measured in acidic electrolytes.[52] Molybdenum phosphide nanoparticles encapsulated in a nitrogen-doped carbon hybrid framework substrate (MoP@NCF) has been synthesized as electrocatalyst via a two-step calcination method.[53] The obtained composite exhibited high electrocatalytic activity in both acidic and alkaline electrolytes, respectively. Ojha et al. synthesized a rGO–MoP composite via two-step programmed pyrolysis using aniline and citric acid as carbon/nitrogen sources.[54] The catalyst could possess overpotentials of 162 mV in 1 M KOH solution and 278 mV in 0.5 M $H_2SO_4$ solution toward HER at current density 10 mA $cm^{-2}$. Li *et al.*[62] prepared a MoP/porous carbon (MoP/PC) composite with well−dispersed/crystallized MoP nanoparticle located in the pores channel of PC through confined growth and in-situ reduction, resulting in a catalyst with both high catalytic activity and stability in acidic and alkaline solution for HER. Liu et al.[63] prepared ultrafine well-crystallized MoP nanoparticles encapsulating in few-layered N, P dual-doped carbon via an electrodeposition process with the assistance of subsequent phosphidation treatment. This electrocatalyst could be utilized as a highly efficient HER performance in a wide pH range due to its high density of active sites, large surface area, high conductivity, and optimized adsorption free energy of H ($\Delta G_{H^*}$). The theoretical calculations by Yan et al.[64] revealed that the coupled interaction between graphitic carbon support and the well-crystallized MoP nanoparticles interfaces played a significant role through fast charge transfer and optimal $\Delta G_{H^*}$ values in enhancing HER performance.

In our work, well-dispersed MoP nanoparticles embedded in 3D N,P−codoped graphite carbon nanosheets (denoted as 3D MoP/NPG) electrocatalyst is succesfully synthesized using a combined space-confined growth and in-situ reduction method. Typically, as illustrated in **Scheme 1**, the porous network precursor is obtained through the confinement effect of $SiO_2$

nanospheres (**I**), and then the unique assembling structure of MoP nanoparticles is anchored on the surface of the obtained carbon sheets through an in-situ reduction method (**II**), resulting in in-situ generation of carbon species coupled with the MoP nanoparticles. Benefiting from abundant active sites, high electrical conductivity, and synergistic effect between MoP and carbon, the catalyst exhibits both remarkable electrocatalytic activity and durability toward HER in a wide pH range.

## 2. Experimental section

### *2.1 Materials*

Tetraethylorthosilicate (TEOS), anhydrous ethanol, ammonium molybdate tetrahydrate [$(NH_4)_6Mo_7O_{24}\cdot 4H_2O$], diammonium hydrogen phosphate [$(NH_4)_2HPO_4$], and ammonium hydroxide (25.0 %～28.0%, GR) were purchased from Sinopharm Chemical Reagent Co., Ltd. Ethylene glycol (EG) was purchased from Adamas Reagent Co. Ltd. Hydrofluoric acid (40 wt.%), Pt/C (20 wt.%) and 5 wt% Nafion® 117 solution were purchased from Sigma−Aldrich Co. Ltd. All the chemical reagents used in the experiments were used without further purification.

### *2.2 Synthesis of $SiO_2$ nanosphere*

Modified Stöber's method was employed to synthesize $SiO_2$ nanosphere.[65] In a typical synthesis, 40 mL of deionized (DI) water was mixed with 55 mL of anhydrous ethanol and 6.8 mL of ammonia (30 wt. %). Then, the mixture solution was stirred for 30 minutes and defined as A. 9 mL of anhydrous ethanol was mixed with 5 mL of TEOS and stirred for 30 minutes, donated as B. Afterwards, B solution was quickly added into A solution with a continuous stirring. The resultant solution was stirred for another 4 hours at room temperature to obtain a milky white suspension, indicating the formation of $SiO_2$ nanospheres. This white suspension were centrifugated and washed several times with ethanol and distilled water to obtain the a powder

of $SiO_2$ nanospheres which were measured to have an average diameter of approximately 100 nm (**Figure S1a** and **S1b**) after dried at 60 ºC for overnight.

*2.3 Synthesis of 3D MoP/NPG*

Typically, 500 mg of $SiO_2$ nanospheres were re−dispersed in DI water (8 mL) and ethylene glycol (2 mL) mixture solution under ultrasonication for about 1 hour to obtain a white mixture. Mo source (120 mg) and P source (96 mg) were dissolved in deionized water (2 mL) and stirred for another 30 minutes. Afterwards, the mixture containing Mo and P was slowly dropped into the white mixture of $SiO_2$ nanospheres dispersed solution under stirring. After continuous stirring for another 2 hours at room temperature, the obtained mixture was evaporated into a slurry at 80 ºC water bath with continous stirring. This slurry was dried at 120 ºC oven for overnight to obtain a light blue powder. Then, this blue powder (400 mg) was placed in a porcelain boat and heated at 700 ºC about 5 hours under Ar atmosphere with the heating rate of 5 ºC $min^{-1}$ and then naturally cooled to room temperature to obtain black powder. This powder (250 mg) was then immersed in 10 mL of 0.5 M HF aqueous solution to remove the $SiO_2$ templates at room temperature. After washed with DI water several times and dried at an oven, the black powder was obtained. The black powder (100 mg) placed in a porcelain boat together with $(NH_4)_2HPO_4$ (100 mg) was heated at 850 ºC under $H_2$(5%)/Ar atmosphere for 150 minutes with a heating rate of 5 ºC $min^{-1}$ and then naturally cooled down at room temperature to obtain a product of 3D MoP/NPG.

*2.4 Synthesis of MoP/C*

Typically, 120 mg of Mo source and 96 mg of P source were dissolved in water/EG (v/v=5:1) mixture solution with stirring for 30 minutes and then dried at 120 ºC drying oven to obtain a powder. This homogeneous mixed powder was placed in a porcelain boat, then heated at 850 ºC under $H_2$(5%)/Ar flowing for 150 minutes with a heating rate of 5 ºC $min^{-1}$ to obtain MoP/C sample.

*2.5 Synthesis of bulk MoP*

Ammonium molybdate (120 mg) and $(NH_4)_2HPO_4$ (96 mg) were dissolved in 10 mL of water with stirring for 30 minutes and then dried at 120 ºC dry oven to obtain a powder. This homogeneous mixed powder was placed in a porcelain boat, and heated at 850 ºC under $H_2$(5%)/Ar ambient for 150 minutes with a heating rate of 5 ºC $min^{-1}$ to obtain the bulk MoP sample.

*2.6 Characterizations*

The morphologies and structures of the as−prepared samples were characterized by scanning electron microscopy (SEM, Hitachi S−4800, 10 kV) and transmission electron microscopy (TEM, JEM−2010F, 200 kV). The Raman spectra were recorded on a Renishaw spectrometer with a laser line of 532 nm. The specific surface area of the as−synthesized catalysts were measured on a Belsorp−max surface area detecting instrument with $N_2$ physisorption at 77 K. The X−ray photoelectron spectroscopy (XPS) spectra of samples were performed on a Thermo VG ESCALAB250 X−ray photoelectron spectrometer with Al Kα radiation. X−ray powder diffraction patterns were taken on a Shimadzu 6000 diffractometer (Cu Kα1, λ= 0.15406 nm).

*2.7 Electrochemical measurements*

All the electrochemical measurements were carried out using a typical three−electrode electrochemical workstation (CHI660E, China). The Pt wire and an Ag/AgCl electrode were used as the counter electrode and the reference electrode, respectively. 4 mg catalysts were dispersed in 1.0 mL of water/Isopropyl alcohol/Nafion (v/v/v=80:15:5) with ultrasonic−assisted for 40 minutes. For working electrode preparation, 5 uL of the well−dispersed catalyst inks was coated on the glassy carbon disk electrode with a diameter of 3 mm to reach a catalyst loadings of 0.28 mg $cm^{-2}$. Prior to electrochemical characterizations, the electrolyte was purged with pure $N_2$ to remove the resolved oxygen and the iR−compensation was applied by using the CHI software. Polarization datas were collected at a scan rate of 5 mV $s^{-1}$ in several electrolytes including 0.5 M $H_2SO_4$ solution, 1.0 M phosphate buffer solution (PBS) and 1.0 M KOH solution. All the potentials, measured against a saturated Ag/AgCl electrode, were converted

into the reversible hydrogen electrode (vs RHE) according to the following equation: $E_{(RHE)} = E_{(Ag/AgCl)} + E^{0}_{(Ag/AgCl)} + 0.059\ pH$.[53] Cyclic voltammogram (CV) was used to investigate the cycling durability for HER at a scan rate of 100 mV $s^{-1}$ for 3,000 cycles in various electrolytes. The long−term stability was tested by the chronoamperometry method at controlled overpotentials. Electrochemical impedance spectroscopy (EIS) measurements were tested from 1 MHz to 0.1 Hz with an AC perturbation voltage of 5 mV.

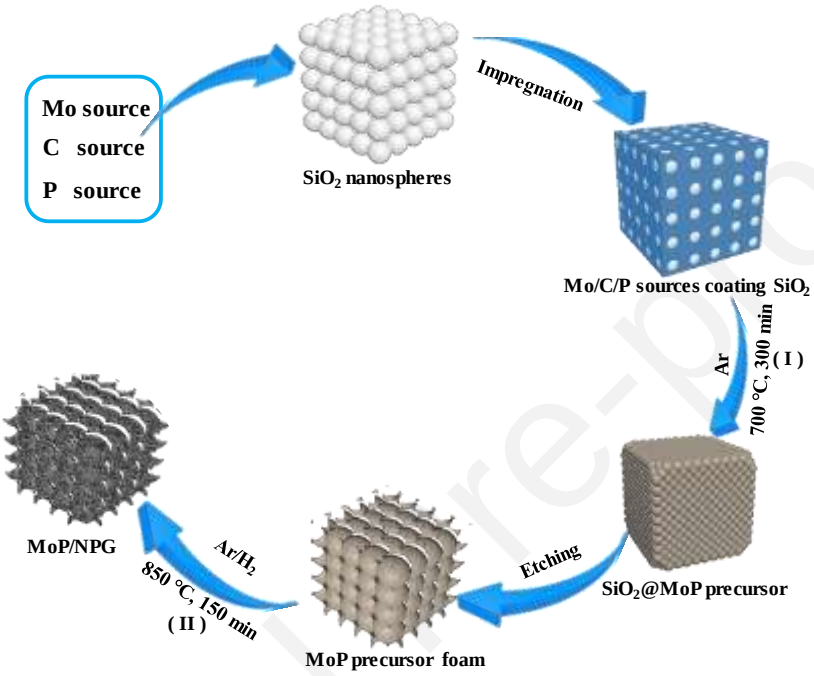


**Scheme 1.** Schematic illustration of the MoP/NPG catalyst synthesis process.

## 3. Results and discussion

The synthetic process of 3D MoP/NPG electrocatalyst is illustrated in **Scheme 1**. Specificlly, the catalyst precursor forms uniformly porous network due to the confined effect of the $SiO_2$ template, as shown in **Figure 1a** and **1b**. The resulting electrocatalyst maintains the network morphology but its surface becomes rough (**Figure 1c**) because the carbon substrate acts as a stablizer to prevent the structure agglomeration. The specific surface areas and porous structures of catalysts can be confirmed by $N_2$ adsorption–desorption isotherms as shown in **Figure 1d**. The BET surface areas (pore volume) of pure MoP and MoP/C are 2.50 $m^2\ g^{-1}$

(0.0055 $cm^3$ $g^{-1}$) and 11.41 $m^2$ $g^{-1}$ (0.025 $cm^3$ $g^{-1}$), respectively. The specific surface area of the MoP/NPG composite is increased dramatically up to 94.49 $m^2$ $g^{-1}$ with a pore volume of 0.22 $cm^3$ $g^{-1}$ due to the confined effect of the hard templates.[66] Without adding the $SiO_2$ template, the rod−shaped catalyst can be obtained, as shown in **Figure S1a** and **S1b**. The catalyst tends to form irregular particle without adding carbon source and hard-templates $SiO_2$, as displayed in **Figure S1c** and **S1d**. Compared with the specific surface area of MoP/NPG hybrid (94.49 $m^2$ $g^{-1}$), the MoP/NPG precursor possesses a higher surface area 109.41 $m^2$ $g^{-1}$ and pore volume of 0.24 $cm^3$ $g^{-1}$ (**Figure S2**) because of the agglomeration of MoP/NPG during the reduction process. According to IUPAC classification, the precursor and the catalyst can achieve the distinct $H_4$−tpye hysteresis loop (at $P/P_0$ = 0.45–1.0) for their mesoporous structure nature.[67-69] Whereas the pure MoP and MoP/C sample just show the typical $H_3$−type hysteresis loop (at $P/P_0$=0.8–1.0) for their porous structure caused by the disordered stacked nanoparticles.[70] Powder XRD patterns of the as-prepared samples are displayed in **Figure 1e**. The characteristic peaks located at around 27.9°, 32.3°, 43.1°, 57.4°, 57.9°, 64.9°, 67.0°, 67.8°, and 74.3° can be attributed to the diffraction of (0 0 1), (1 0 0), (1 0 1), (1 1 0), (0 0 2), (1 1 1), (2 0 0), (1 0 2), and (2 0 1) planes of hexagonal MoP (JCPDS No. 24−0771), respectively.[19,71] A broad and weak peak can be detected at around 26° in MoP/NPG sample (**Figure 1e** (**iii**)), which is indicative of the (0 0 2) plane of the graphite carbon coming from the EG carbonization.[72] Mo−based oxides are obtained after the first−step pyrolysis, which can be detected by XRD measurement as shown in **Figure S4a**. Raman spectrum confirms the existence of graphite carbon in MoP/NPG sample (**Figure S3**), which is in agreement with the above-mentioned XRD analysis. The Raman spectra of MoP/NPG and MoP/C appear two peaks at around 1361 and 1587 $cm^{-1}$, corresponding to the D band and G band, respectively. The D band is contributed to the defects and the $sp^3$-hybridized carbon atoms in carbon structure, while the G band is ascribed to hexagonally bonded $sp^2$-carbon atoms in the graphitic networks. Raman spectrum of MoP/NPG exhibits a high graphitization degree with a ratio of D band to

G band ($I_D/I_G$) of 1.02) due to the two-step programmed pyrolysis. The above results demonstrate that the carbonization and phosphorization processes can successfully promote the MoP/carbon precursor to convert into MoP/NPG catalyst.

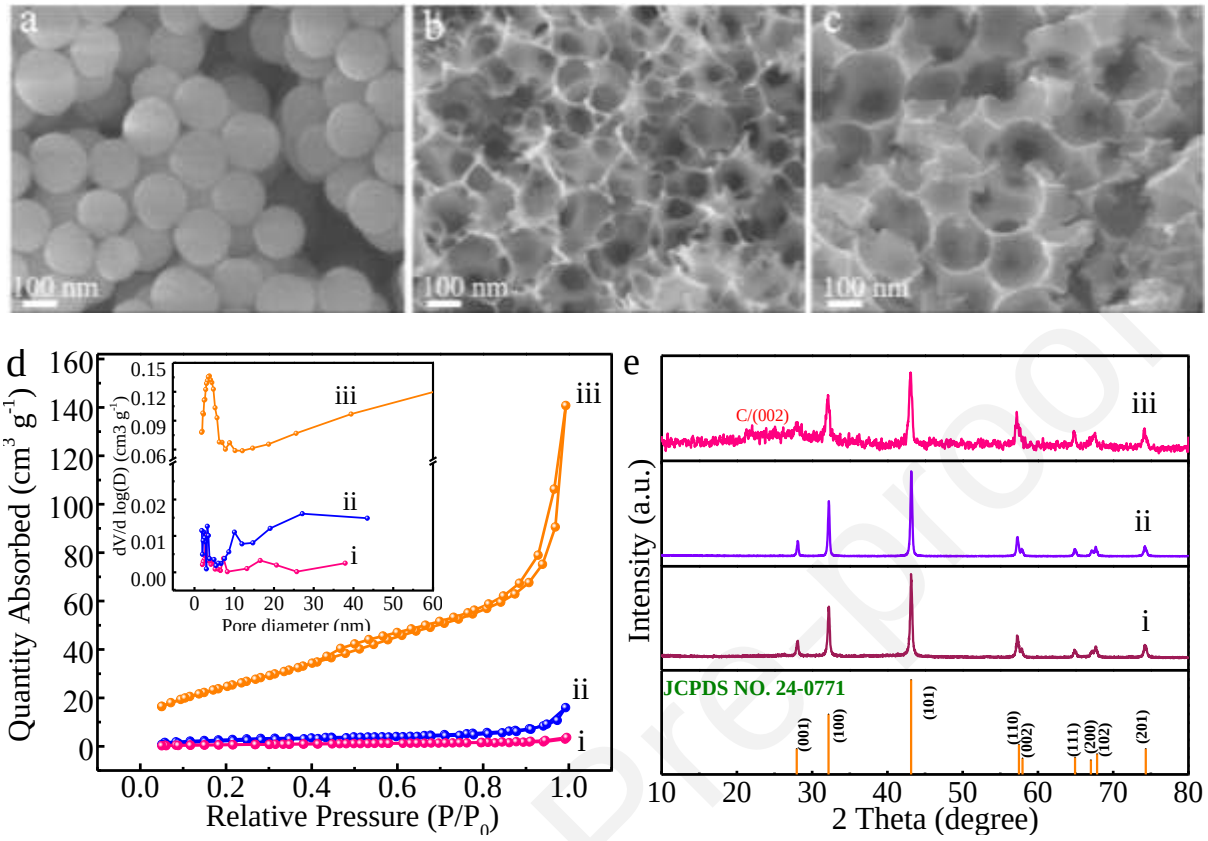


**Figure 1.** SEM images of (a) $SiO_2$ nanospheres, (b) 3D MoP/NPG persorcur and (c) the 3D MoP/NPG catalyst. (d) $N_2$ adsorption−desorption isotherms of the samples: (i) bulk MoP, (ii) MoP/C and (iii) 3D MoP/NPG catalysts. (Insets: The pore size distributions of the samples). (e) XRD patterns of the pure (i) MoP, (ii) MoP/C and (iii) 3D MoP/NPG catalysts.

**Figure 2** displays the morphology and components of the sample observed by TEM and energy-dispersive X-ray (EDX) analysis, respectively. TEM images of 3D MoP/NPG catalyst reveal that MoP nanoparticles with an average diameter of ~5 nm uniformly, which are anchored in the pore channels of carbon layers (**Figure 2a** and **2b**). HRTEM images exhibit the well-resolved lattice spacings of 0.210 nm and 0.271 nm (**Figure 2c** and **2d**), corresponding to the (1 0 1) and (1 0 0) planes of MoP, respectively. The missing lattice fringes in **Figure 2d**

suggest the existence of defects in the MoP crystals. Such structural defects are likely to offer more unsaturated active atoms, which can modulate the electronic configuration and in turn tune the activity of active sites to improve the catalytic activity. EDX mappings of the MoP/NPG catalyst (**Figure 2e**) reveal the distribution of elements, including molybdenum, phosphorus, nitrogen, carbon, and oxygen in the 3D porous network architecture. The O element signal should be attributed to the organic carbon source and the surface oxidation of MoP nanoparticles. The overlapping element signals confirm the hierarchical structure composed of MoP and heteroatom-doped carbon layer.

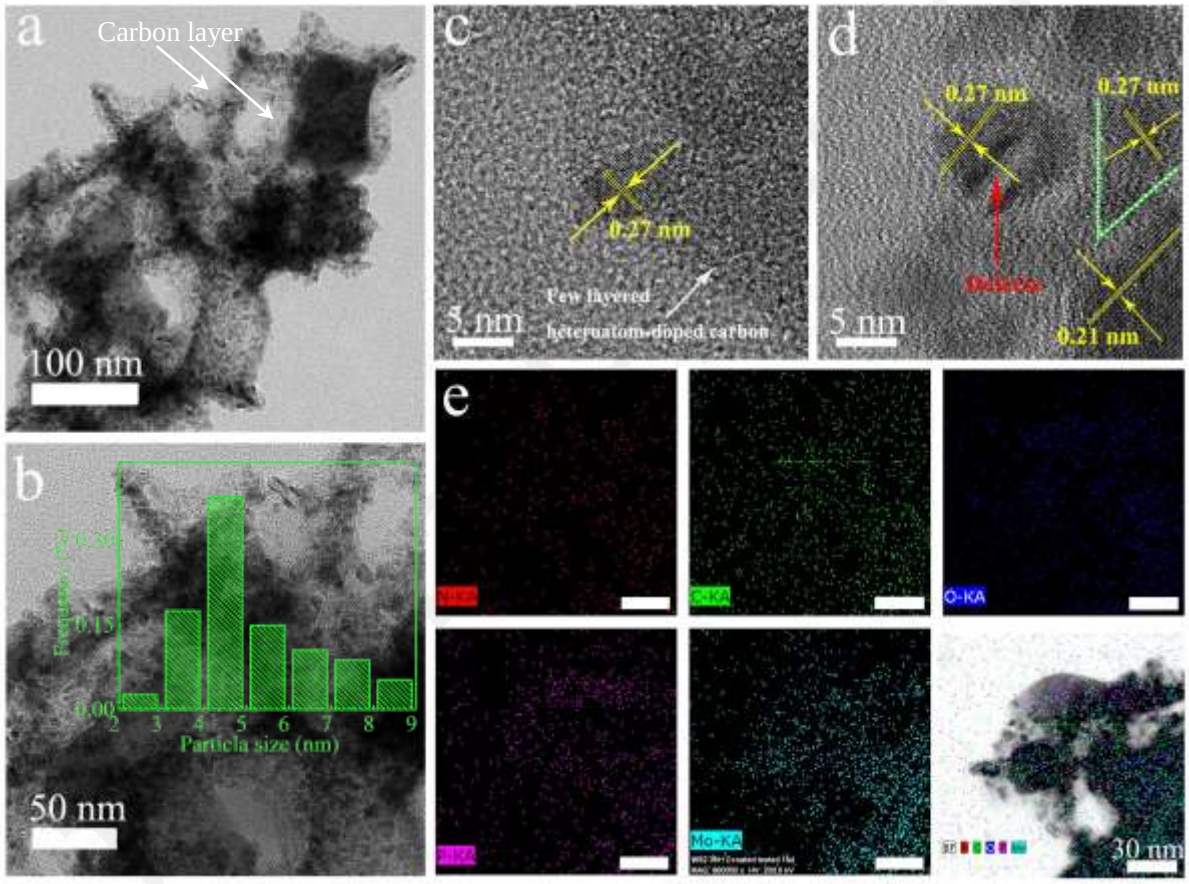


**Figure 2.** (a, b) TEM images and (c, d) HRTEM images of 3D MoP/NPG catalyst. The inset image of (b) shows the corresponding particle size distribution of MoP nanoparticles embedded in few layered carbon. (e) The EDX elemental mapping images and the overlay image of the 3D MoP/NPG catalyst.

X−ray photoelectron spectroscopy (XPS) was used to analyse the composition and valence states of the elements in MoP/NPG catalyst. Survey spectrum (**Figure 3a**) suggests the existence of Mo, P, C, O and N, which are consistent with the results of the EDX analysis. **Figure 3b** and **3c** exhibit the high−resolution XPS spectra of Mo 3d and P 2p. The peaks at 228.2 eV and 231.4 eV in Mo 3d XPS spectrum can be assigned to $Mo^{\delta+}$ species ($0 < \delta < 4$), which are the typical peaks ascribed to MoP.[73-75] The binding energies at 232.0/235.4 eV and 233.0/236.2 eV can be assigned to the $MoO_2$ and $MoO_3$ species, respectivity.[76] The $MoO_x$ species should be derived from the inevitable oxidation of the MoP surface during air exposure.[74] The deconvoluted P 2p profiles clearly show the two peaks at 129.3 and 130.2 eV corresponding to the $P^{\delta-}$ species in MoP. The peaks located at 133.2 and 134.0 eV (**Figure 3c**) can be assigned to the binding energies of P−C and P−O, respectively.[63] The peak at 134.0 eV should be attributed to the surface oxidation species (such as $PO_4^{3-}$) due to the air contact.[63] The XPS spectrum of O 1s (**Figure 3d**) can be deconvoluted into three peaks, i.e., P−O (533.2 eV), C−O (531.9 eV), and Mo−O (530.5 eV).[77] The C 1s spectrum (**Figure 3e**) shows a strong peak at 284.5 eV ascribing to C=C/C−C species, and a relatively weak peak at 285.6 eV to the C–P/C−N species.[75] The formation of P–C species reveals the successful incorporation of P into graphitic carbon layers. As shown in **Figure 3f**, the peaks appears at 398.7, 400.1 and 401.6 eV, which are corresponding to pyridinic−N, pyrrolic−N, and graphitic−N species, respectively.[63] The peak at 394.2 eV in N 1s spectrum can be donated to the Mo–N coupling phase, known as the catalytic sites for HER.[78] The formation of Mo-N species reveals that N also tends to modify the surface of MoP nanoparticles. The content of N species in 3D MoP/NPG catalyst is calculated to be 1.61 at% (**Figure S4c**). The presence of N/P dopants is expected to improved HER activity through the synergistic effects of MoP and N,P-codoped carbon layers due to the increased electron density in graphitic carbon layers.[64]

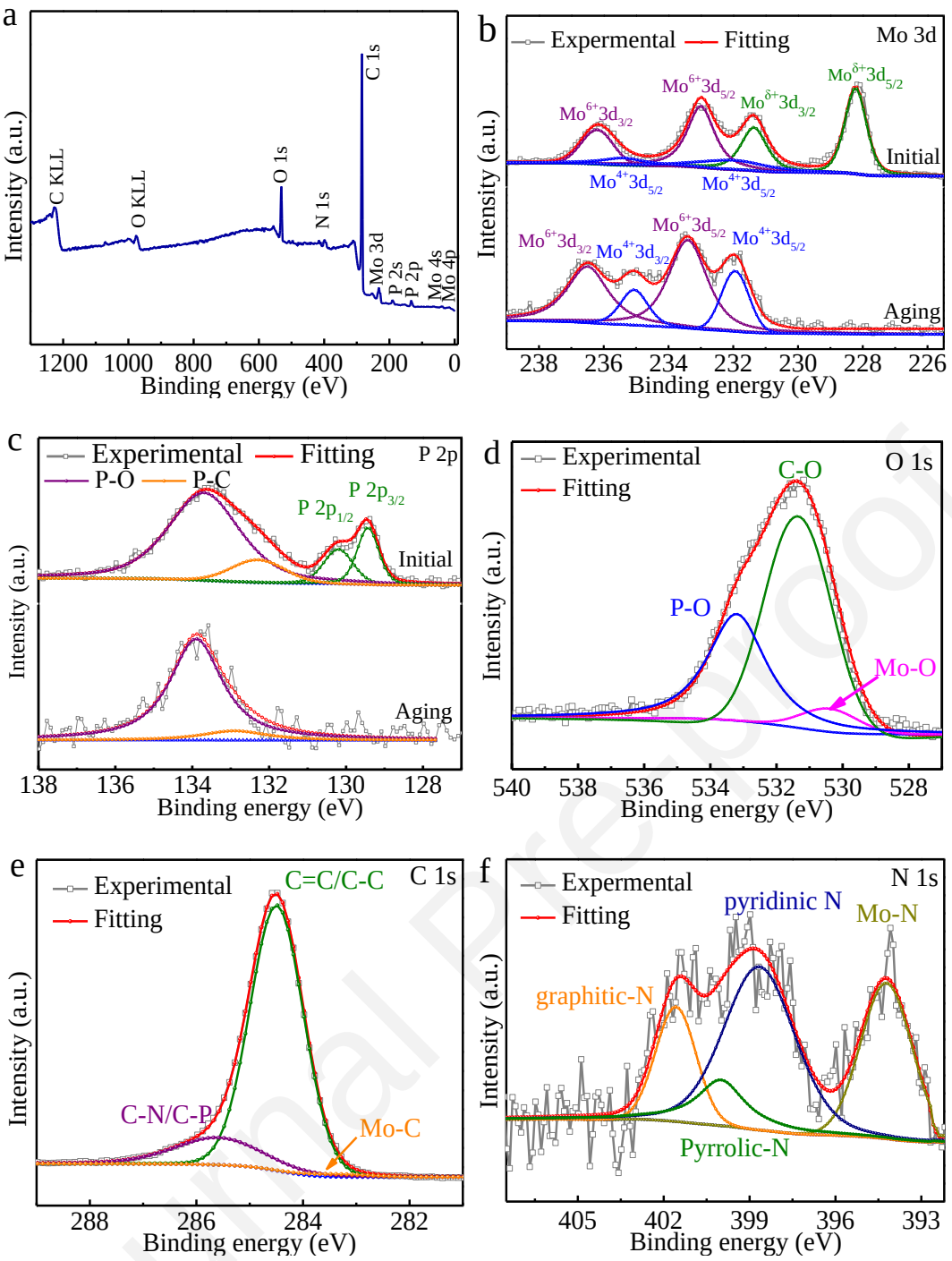


**Figure 3.** Surface composition and chemical state analysis of MoP/NPG catalyst: (a) XPS full spectrum; high−resolution spectra of (b) Mo 3d, (c) P 2p, (d) O 1s, (e) C 1s and (f) N 1s. The aging effects in air are also shown in the lower panels in (b) and (c).

It should be noted that the characteristic peaks of MoP are disappeared after aging several days in air (**Figure 3b** and **3c**). For Mo 3p spectrum, the obtained peaks are ascribed to $MoO_2$ and

$MoO_3$, respectively (**Figure 3b**). For P 2p, the signals of MoP dissapeared as shown in **Figure 3c,** except for the binding energies of P−O and P−C. Meanwhile, XRD measurement has revealed the well−crystallized MoP in the MoP/NPG catalyst due to its high detective depth comparing to XPS technique. There are no obvious peaks belonging to the $MoO_2$/$MoO_3$ as observed in **Figure 1e**(**iii**).

Electrochemical measurements were performed in $N_2$-saturated 0.5 M $H_2SO_4$ aqueous solution to verify the electrocatalytic performance of the prepared catalysts toward HER. The pure MoP shows the current density of 10 mA $cm^{-2}$ at the overpotential of 385 mV with an onset potential of 264 mV, as shown in **Figure 4a**. The catalytic activity of the MoP/C catalyst shows a better activity with a small overpotential of 219 mV triggering the current density of 10 mA $cm^{-2}$ with an onset potential of 160 mV. However, MoP/NPG catalyst shows even lower overpotential (148 mV) to achieve current density of 10 mA $cm^{-2}$ with an onset potential of 96 mV, and the $H_2$ bubbles could be observed on the surface of MoP/NPG modified electrode (**Figure S5a**). This higher catalytic HER activity of MoP/NPG can be attributed to its abundant active sites and the accelerated diffusion reactants within the 3D MoP/NPG layer.

The Tafel slopes of the prepared catalysts were calaculated from the polarization curve by the correlated Tafel equation ($\eta$=a + b log |j|, j is the current density, b is the Tafel slope), as shown in **Figure 4b**.[79] The Pt/C catalyst gives the lowest Tafel slope (30 mV $dec^{-1}$) as the reference. The Tafel slope of MoP/NPG (49 mV $dec^{-1}$) is lower than those of MoP/C (61 mV $dec^{-1}$) and pure MoP (127 mV $dec^{-1}$), which is in good agreement with the higher HER activity. As compared with the previous reported state−of−the−art Mo−based non−noble metal HER catalysts (**Table S1**), the 3D MoP/NPG catalyst exhibits the competitive catalytic activity in 0.5 M $H_2SO_4$ electrolyte. Normally, the value of Tafel slope can be used to indicate the rate−limiting step toward HER. For HER three principal steps are possibly involved in different electrolytes, including the Volmer step ($H^+ + e^- \rightarrow H^*$ in acidic solution; $H_2O + e^- \rightarrow H^* + OH^-$ in neutral and basic solution), Heyrovsky step ($H^* + H^+ +$

$e^- \rightarrow H_2$ in acidic solution; $H_2O+e^-+H^* \rightarrow H_2+OH^-$ in neutral and basic solution) and Tafel step ($H^*+H^* \rightarrow H_2$). In our case, the Tafel slope of the MoP/NPG catalyst is 49 mV $dec^{-1}$, suggesting that the release of molecular hydrogen is the rate determining step and the hydrogen evolution process follows the Volmer−Heyrovsky mechanism,[80] as illustrated in **Scheme 2a**. Furthermore, the Heyrovsky−step may be optimized by the porous structure to generate a significant improvement of the HER reaction rate in comparation with the MoP/C and pure MoP catalysts.

The exchange current density ($j_0$) of the catalysts (**Table S2**) was estimated by extrapolating the Tafel plots, as shown in **Figure S5b.** The 3D MoP/NPG catalyst has a higher exchange current density than those of MoP/C and pure MoP in acidic solution. Electrochemical impedance spectroscopy (EIS) was employed to illustrate the charge transfer kinetics at the cathode electrode/electrolyte interface immersed in typical electrolytes.[63] The Nyquist plots of the as-prepared catalysts can be observed in **Figure 4c**. A simplified equivalent circle, as shown in **Figure S6**, is used to fit the half circle and the corresponding resistance parameters obtained are listed in **Table S3**. The MoP/NPG catalyst exhibits a lower charge transfer resistance (13.3 Ω) than that of the MoP/C (19.8 Ω) and pure MoP (64 Ω), suggesting that the 3D porous structure can give a higher charge transfer kinetics. Cyclic voltammetry (CV) method was used to evaluate the electrochemically active surface area (ECSA) of the samples (**Figure S7**). As illustrated in **Figure 4d**, the $C_{dl}$ value of 3D MoP/NPG catalyst (13.9 mF $cm^{-2}$) are two times and nine times higher than those of MoP/C (6.5 mF $cm^{-2}$) and pure MoP (1.6 mF $cm^{-2}$), respectivity. No obvious decay can be observed comparing to the initial polarization curve of the working electrode with the 3000$^{th}$ sweep curve, showing the excellent stability of MoP/NPG catalyst (**Figure 4e**). This high stability may be resulted from high 3D nanostructural stability and the strong interaction between MoP nanosheets and carbon sheets. The chronoamperometric electrolysis at an overpotential of 180 mV for 60 hours still maintains high

catalytic performance (Insert of **Figure 4e**). The slightly increased current density (60 hours) may be attributed to the diffusion of the dissolved Pt ion during the chronoamperometric process. **Figure 4f** shows a quick response current for the MoP/NPG catalyst because the 3D porous structure with well-dispersed active sites can provide rapid pathways for ionic diffusion and fast charge transfer. Therefore, benefiting from the large specific surface area with abandunt active sites, high electrical conductivity, and the synergistically coupled interaction, the 3D MoP/NPG electrocatalyst can possess higher HER activity than the other prepared catalysts.

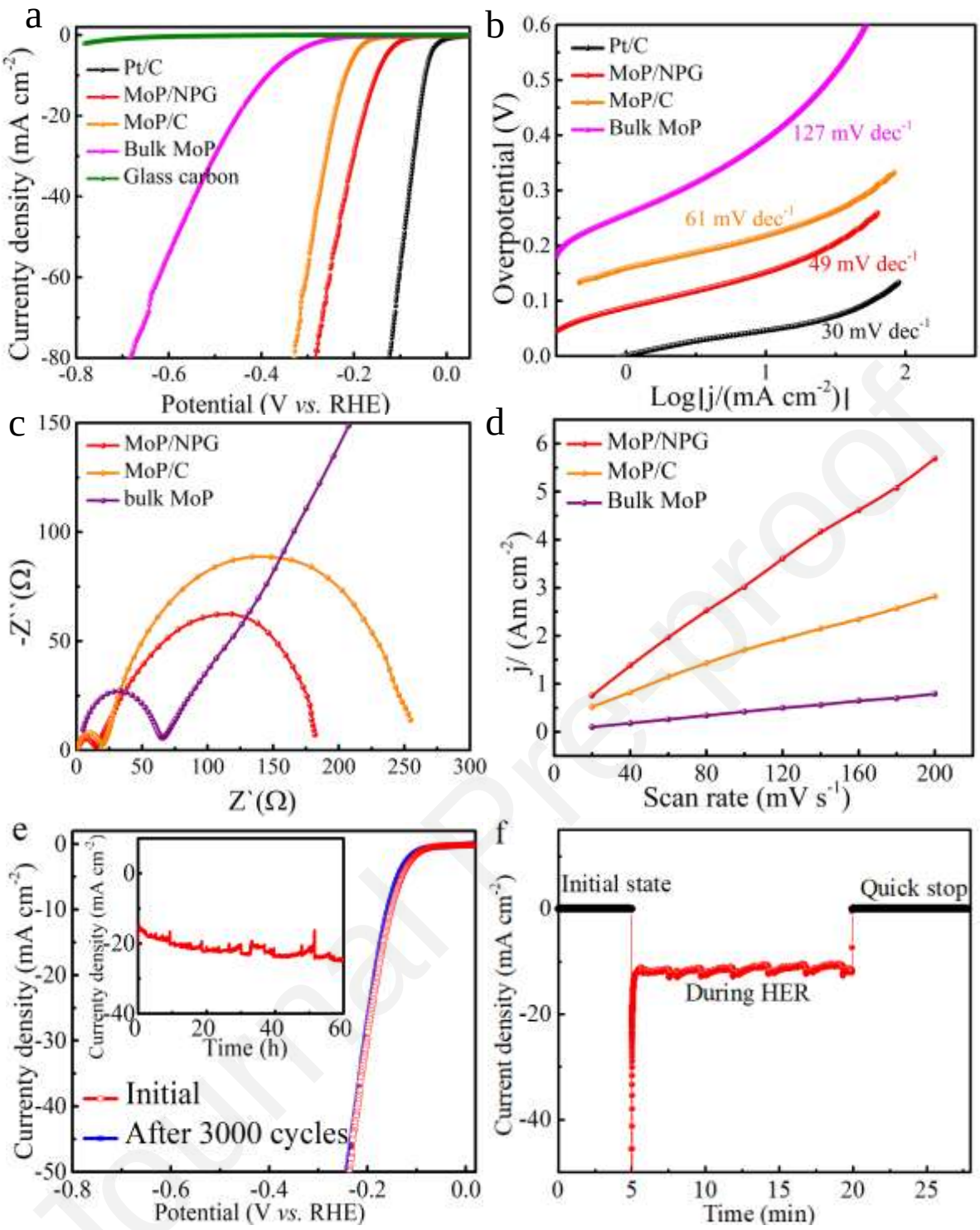


**Figure 4.** (a) Polarization curve of MoP/NPG in 0.5 M $H_2SO_4$ solution with a scan rate of 5 mV $s^{-1}$, comparing with those of Pt/C, MoP, MoP/C and the bare glass carbon electrode. (b) Tafel plots of the prepared catalysts. (c) Electrochemical impedance spectra of the catalysts at an overpotential of 180 mV in 0.5 M $H_2SO_4$ electrolyte. (d) The capacitive current at 0.15 V as a function of scan rate for various catalysts. (e) Polarization curves of MoP/NPG initially and

after 3000 cycles in 0.5 M $H_2SO_4$ electrolyte at a scan rate of 5 mV $s^{-1}$. Insets: Time−dependent current density curves of MoP/NPG under static overpotential of 180 mV for 60 hours. (f) The electrochemical performance of MoP/NPG in the states of initial, during HER and quick stop from HER in 0.5 M $H_2SO_4$ solution.

The catalytic activities of MoP/NPG electrocatalyst were also measured in neutral and alkaline electrolytes, respectively. The MoP/NPG catalyst shows high catalytic activity in 1.0 M PBS solution with an overpotential of 150 mV at current density of 10 mA $cm^{-2}$ with a Tafel slope of 102 mV $dec^{-1}$ in neutral electrolyte, as shown in **Figure 5a**. The MoP/NPG catalyst also exhibits a small overpotential of 126 mV at the current density of 10 mA $cm^{-2}$ with a Tafel slope of 56 mV $dec^{-1}$ in the extreme alkaline solution (**Figure 5b**), which is competitive to the previous reported Mo−based non−noble metal HER catalysts (**Table S4**) in alkaline electrolyte. The obtained hierarchical porous structure contributes to the efficiency of liquid-solid-gas three-phase interfacial conversion, facilitates the transport of reaction intermediates and release of hydrogen during electrochemical process, which is beneficial for smoothing the Heyrovsky step.[27] The outstanding catalytic activity for HER in alkaline solution should derive from hierarchical porous structure, high density of exposed active sites and synergistic interaction between MoP nanoparticles and carbon sheets in the hybrid. The 3D MoP/NPG are stable in both neutral and alkaline media (**Figure 5c-5f**) after continuous 3000 CV cycles (**Figure 5c, 5d**). The current densities of 3D MoP/NPG can maintain a long-term durability electrolysis for at least 30 hours in 1.0 M PBS and 12 hours 1.0 M KOH solution while a fixed overpotential is applied (Figure **5e, 5f**). It should be noted that the activity of MoP/NPG catalyst in alkaline electrolyte is slightly higher than that in acidic solution because more active sites can be exposed to the alkaline electrolyte due to the dissolution of oxidized surface species ($MoO_x$) in alkalic solution, as reported by Tang *et al*.[81] The possible catalytic mechanism on the surface of porous structural MoP measured in neutral/alkaline electrolytes toward HER is illustrated in

**Scheme 2b**. It is believed that the coupled interaction beween carbon matrix and MoP with optimum binding strength to $H_2O$ and $OH_{ad}$ can facilitate the adsorption and dissociation of $H_2O$ to supply $H_{ad}$ to the nearby active sites on the surface of MoP, while the carbon matrix is beneficial to the electron transfer, H adsorption, combination of H intermediates and desorption of $H_2$ through a Heyrovsky step. The large specific surface area of 3D structural MoP/NPG catalyst with more active sites can further optimize the multi−step electrochemical reaction processes involving liquid−solid−gas three−phase interface behaviors. The MoP/NPG catalyst prefers the acidic and neutral electrolytes rather than alkaline solution, as indicated by the comparison of cyclic voltammetry (CV) durability and the long−term electrochemical durability of MoP/NPG catalyst toward HER in acidic, neutral and alkaline solution, which may be attributed to the perishable ultrathin structure with high surface area in alkaline solution as previously reported Mo−based catalysts in alkaline electrolyte.[72,81,82] The MoP/NPG catalyst possesses a high catalytic activity and durability in a wide pH range, which are comparable to those of noble metal catalyst (Pt/C), as shown in **Figure 5** and **Figure S8,** and listed in **Table S5**. The chronoamperometry respond curves are fluctuated up and down due to the bubble formation and release over continuing for 60, 30 and 12 hours, respectively. All the above results further demonstrates that the coupled interaction between MoP/NPG interfaces can facilitate the charge transfer and optimize the reaction intermediates, results in excellent catalytic activity and durability for HER in a wide pH range.

EIS measurements were further performed to understand the HER activity dependency on pH values. Nyquist plots of the 3D MoP/NPG catalyst, as shown in **Figure S9**, suggest a two−time constant process under various electrolytes. Estimated by using the simplified equivalent circle (**Figure S6)**, the charge transfer resistances are 13.3 Ω in acidic, 11.5 Ω in alkaline, and 43.7 Ω in neutral media. The series resistance are 1.0 Ω, 2.0 Ω, and 2.7 Ω in the corresponding electrolytes, respectively, indicating high conductivity and fast charge transfer rate (**Table S6**). The curvature radius of semicircular has a weak enhancement following the enhanced applied

overpotential at high frequency, which should be ascribed to the interfacial charge transfer and responsible for the formation of bubbles at a higher overpotential hindering the intimate contact between electrolyte and electrode. The radius of semicircular at low frequency region becomes smaller with increasing overpotential for the enhanced HER kinetics.[83] The 3D MoP/NPG catalyst in alkaline electrolyte has a lower charge transfer resistance than that in acidic solution, suggesting a good catalytic performance in alkaline medium. A larger electrochemical surface area (**Figure S10 and Table S7**) can also contribute to the enhanced catalytic performance in alkaline solution. The measured $C_{dl}$ is 14.1 mF $cm^{-2}$ in alkaline electrolyte, 13.9 mF $cm^{-2}$ in acidic electrolyte, and 12.3 mF $cm^{-2}$ in neutral electrolyte. The catalytic activity of catalyst can be further demonstrated by the hydrogen turnover frequency (TOF). **Figure S11a** shows the TOF curves of catalysts, indicating that the 3D MoP/NPG catalyst possesses higher intrinsic HER activity. The high density of active sites and strong interaction between the MoP and carbon substrate induce synergistic effect to optimize the adsorption/desorption of hydrogen intermediate. TOF results also reveal that the 3D MoP/NPG catalyst in alkaline solution can realize the maximum intrinsic HER activity (**Figure S11b)**. The high catalytic activity is attributed to the high density of the exposed MoP active sites. The $MoO_x$ species on the surface of MoP would result in low activity of active sites and low density of active sites, which are in agreement with the analysis of electrochemical active surface area (ECSA) and TOF results. As observed in **Figure S12**, the Mo 3d and P 2p XPS spectra of as-prepared MoP/NPC catalyst have no obvious change in terms of peak position after long-term durability tests in both acidic and neutral media, suggesting high stability of the catalyst for HER. The MoP characteristic peaks disappeared after long-term durability tests in 1 M KOH solution, which are consistent with those of MoP/NPC after aging several days. Surface $MoO_x$ species could only be detected by XPS technique due to its low detective depth. Moreover, XRD spectra (**Figure S13**) also reveal that the MoP/NPC hybrid remains the crystal structure after long-term durability test in various electrolytes, indicating high catalytic stability of MoP/NPC catalyst over a wide pH range. These results demonstrate

that the 3D MoP/NPG catalyst has high electrocatalytic activity and stability toward HER in a wide pH range.

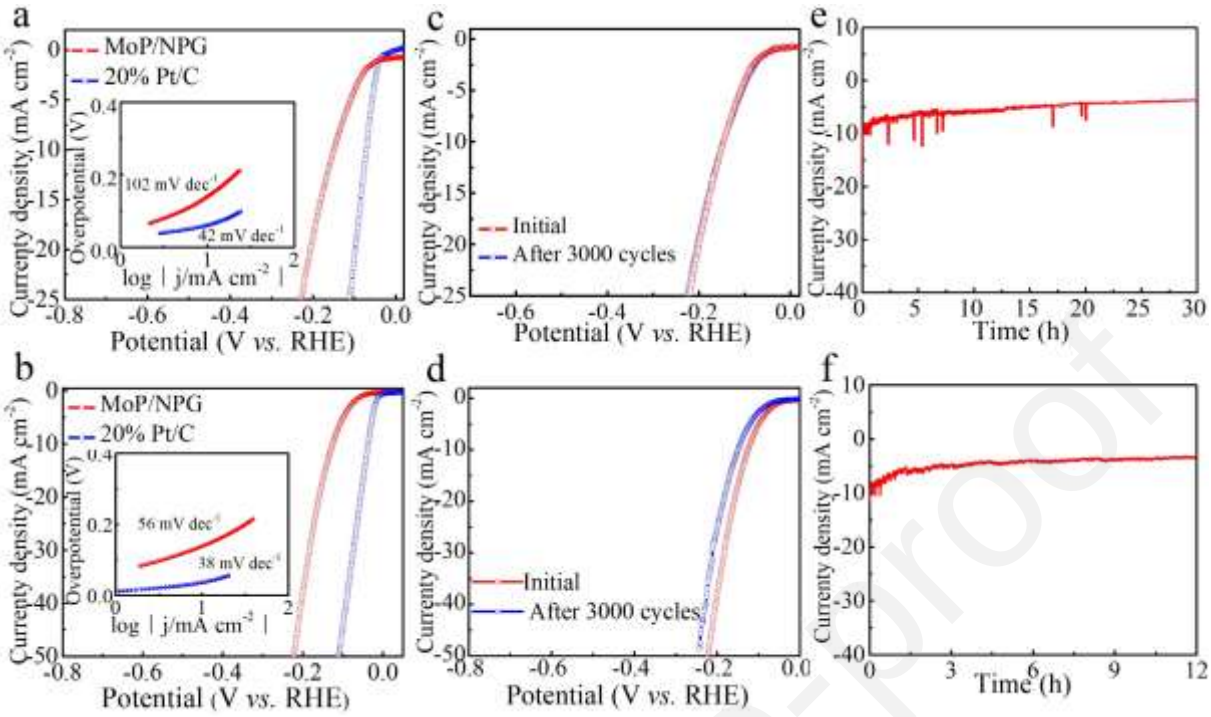


**Figure 5.** (a) Polarization curves of MoP/NPG, along with that of 20 wt% Pt/C for comparison in 1 M PBS electrolyte. (Insets: the corresponding Tafel plots of MoP/NPG and Pt/C.) (b) Polarization curves of MoP/NPG catalyst, along with that of 20 wt.% Pt/C for comparison in 1 M KOH electrolyte. (Insets: the corresponding Tafel plots of MoP/NPG and Pt/C.) (c) Cycling stability of MoP/NPG before and after 3000 cycles in 1 M PBS electrolyte. (d) Cycling stability of MoP/NPG before and after 3000 cycles in 1 M KOH electrolyte. (e) The time−dependent current density curve under a static overpotential for 30 hours in neutral solution. (f) The time−dependent current density curve of MoP/NPG under a static overpotential in alkaline solution. Scan rate: 5 mV $s^{-1}$.

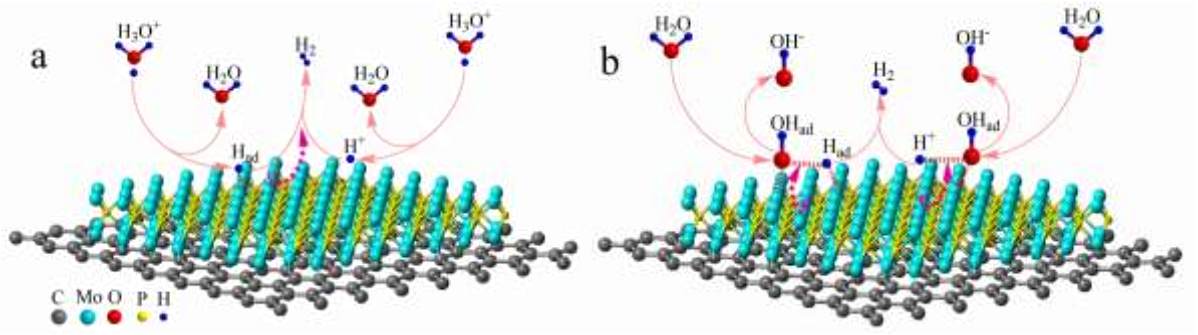


**Scheme 2.** Possible catalytic mechanism on the surface of 3D MoP/NPG catalyst toward HER. Schematic showing HER processes occurred on the surface of 3D MoP/NPG catalyst in acidic (a) and neutral/alkaline media (b).

Density functional theory-based calculation of the surface chemistry of MoP nanosheet and their coupling mechanism to the graphite carbon nanolayer is critical in analyzing the interaction nature of hybrid MoP & Graphene nanostructures, which can be used as catalytic surface to adsorb hydrogen atom to further understand their catalytic HER performance. As shown in **Figure S15**, once coupled to graphene, Mo−terminated MoP nanolayer is energetically preferred with much higher binding energy, around 5.90 eV, compared to 0.67 eV in interacted graphene and P−terminated MoP. The stronger coupling strength in the former case can be visualized by the formation of a number of covalent Mo−C bonds in between. Noticeably, a pocket as a result of structural distortion of graphene sheet is formed in the coupled MoP&Graphene hybrid, which may be assistive to the accommodation of hydrogen atoms. The HER activity of coupled MoP&Graphene hybrid was evaluated by the calculation of the adsorption free energy of H ($\Delta G_{H^*}$) on its surface, compared to the results on pure surface of Mo−terminated MoP nanolayer. The adsorption free energy of H, $\Delta G_{H^*}$, on pure MoP and MoP/G hybrid with different H coverage were calculated, the results obtained are shown in **Figure 6a**. As a thumb rule, the electrocatalyst with superior HER performance should have an ideal adsorption free energy of H, $\Delta G_{H^*} \sim 0$. The absolute values of calculated adsorption free energies of H on MoP surface alone are around 0.2 eV at lower H* coverage of 11% and 22%,

but increased to a much high value of 0.8 eV at a 33% H* coverage. This result is consistent with the previously reported experimental results that Mo−terminated MoP nanosheets are ideal choice for HER catalytic reactions for low H coverage rather than that of P−terminated MoP.[52] When MoP monolayer was coupled to graphene, the absolute values of calculated adsorption energies of H are sharply reduced from 0.6 eV for low H* coverage (11%) to 0.2 eV at 22% H* coverage, and most interestingly to a nearly zero value at 33% H* coverage. The adsorption free energy of hydrogen on noble metal Pt has also been simulated, which possessed the low $|\Delta G_{H^*}|$ (0.09 eV). The low $\Delta G_{H^*}$ resulted in high electrocatalytic activity on Pt-based nanomaterials.[9,20] As shown in **Figure 6b** and **Figure S16**, a pocket is formed between MoP monolayer and the graphene layer as a result of strong coupling of these two interacted layers. This pocketed structure provides an open space for an easy accommodation of H atoms especially at high H coverage. N atoms doping in carbon layer of the MoP/NPG catalyst would further increase the electron density on the surface of carbon layer.[25] Our results calculated by DFT indicate that MoP/NPG as a catalyst can give outstanding catalytic activity for HER under high coverage of H, which indicates the indispensable importance of carbon layer to hydrogen evolution reaction.

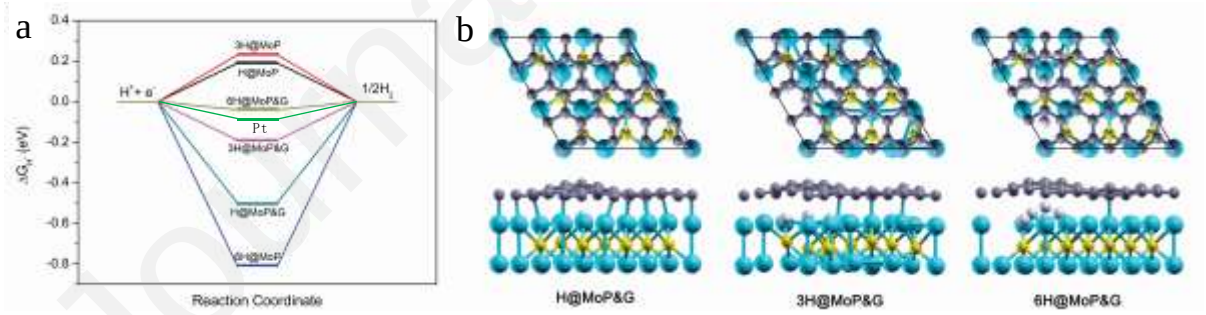


**Figure 6.** (a) Calculated adsorption free energy of hydrogen on the surface of pure MoP and MoP/G hybrid structures for different H coverages. (b) From left to right, two schematic views of the 11%, 22%, and 33% hydrogen covered hybrid structures of graphene on Mo−terminated MoP surfaces, respectively. The cyan, yellow, white, and grey spheres represent Mo, P, H, and C atoms, respectively.

## 4. Conclusions

In the effort to develope more effective electrocataysts for water electrolysis hydrogen generation through hydrogen evolution reaction (HER), the well-crystallized molybdenum phosphide nanoparticles dispersed in three−dimensional N,P−codoped graphite carbon nanosheets (3D MoP/NPG) is synthesized through a $SiO_2$-template-assisted strategy. Benefiting from the catalyst's large specific surface area, high electrical conductivity and coupled interfaces between MoP and carbon sheets, the obtained nano-composite material exhibits a remarkable catalytic HER activity with a small overpotential of 148 mV in 0.5 M $H_2SO_4$, 150 mV in 1.0 M PBS, and 126 mV in 1.0 M KOH electrolytes at current density of 10 mA $cm^{-2}$, respectively. The hierachical porous structure of such a catalyst with abundant active sites and abundant channels for mass transport, and high electrical conductivity ensures the fast electron transfer kinetics for HER. The synergistic interaction between MoP and carbon sheets can modify the electronic structure of the catalyst and accelerate the charge transfer between MoP and carbon sheets interfaces. For fundamental understanding of the catalytic mechanism, density functional theory (DFT) calculations are also carried out, and the results reveal that the coupled interaction between MoP and carbon sheet interfaces can induce an optimal free energy of hydrogen adsorption on the catalyst surface. As demonstrated by both the theoretical calculations and experimental results, the hierarchical structure with a synergistic interaction between MoP and carbon sheets can facilitate reaction kinetics to boost the HER performance. We believe that this work can offer a novel strategy to design high performance electrocatalysts for energy conversion applications to replace the expensive noble metal catalysts.

**Acknowledgements**

This work is financially supported by National Natural Science Foundation of China (Grant No. 51572166), the Shanghai Key Laboratory of High Temperature Superconductors (No. 14DZ2260700), and the Australian Research Council (ARC) Future Fellowship grant (FT160100281). The authors thank the Analysis and Research Center of Shanghai University for their technical support. Wenxian Li acknowledges research support from the Program for Professors with Special Appointments (Eastern Scholar: TP2014041) at Shanghai Institutions of Higher Learning. This research was also undertaken with the assistance of resources from the National Computational Infrastructure (NCI), which is supported by the Australian Government under the NCRIS program.

**Supporting Information**

The Supporting Information is available free of charge on the website at DOI: http://xxx/xxxxx/xxxx.

**References**

[1] F. Yu, H.Q. Zhou, Y.F. Huang, J.Y. Sun, F. Qin, J.M. Bao, W. A. Goddard, S. Chen, Z.F. Ren, Nat. Commun. 9 (2018) 2551.

[2] N. Morlanés, K. Takanabe, V. Rodionov, ACS Catal. 6 (2016) 3092−3095.

[3] C. Liu, B. C. Colón, M. Ziesack, P. A.Silver, D. G. Nocera, Science 352 (2016) 1210−1213.

[4] C. Hu, Y. Xiao, Y. Zou, L. Dai, Electrochem. Energy Rev. 1 (2018) 84−112.

[5] J. Gu, J.A. Aguiar, S. Ferrere, K.X. Steirer, Y. Yan, C.X. Xiao, J.L. Young, M. Aljassim, N.R. Neale, J.A.Turner, Nat. Energy 2 (2017) 16192.

[6] L L.Wang, X. Liu, J.M. Luo, X.D. Duan, J. Crittenden, C.B. Liu, S.Q. Zhang, Y. Pei, Y.X. Zeng, X.F. Duan, Angew. Chem. Int. Ed. 56 (2017) 7610–7614.

[7] Q. Wang, T. Hisatomi, Q. X. Jia, H. Tokudome, M. Zhong, C.Z. Wang, Z.H. Pan, T. Takata, M. Nakabayashi, N. Shibata, Y.B. Li, I.D. Sharp, A. Kudo, T. Yamada, K. Domen, Nat. Mater. 15 (2016) 611.

[8] I.S. Amiinu, Z.H. Pu, X.B. Liu, K.A. Owusu, H. G. R. Monestel, F.O. Boakye, H.N. Zhang, S.C. Mu, Adv. Funct. Mater. 27 (2017) 1702300.

[9] R. Ge, W. Li, J. Huo, T. Liao, N.Y. Cheng, Y. Du, M. Zhu, Y. Li, J. Zhang, Appl. Catal. B: Environ. 246 (2019) 129–139.

[10] D. Kim, D.R.Whang, S.Y. Park, J. Am. Chem. Soc. 138 (2016) 8698−8701.

[11] Q.Y. Jin, B. W. Ren, D.Q. Li, H. Cui, C.X. Wang, Nano Energy 49 (2018) 14−22.

[12] T. Yang, H. Zhu, M. Wan, L. Dong, M. Zhang, M. Du, Chem. Commun. 52 (2015) 990−993.

[13] P. Xiao, Y. Yan, X.M. Ge, Z.L. Liu, J.Y. Wang, X.Wang, Appl. Catal. B: Environ. 154–155 (2014) 232−237.

[14] J. Lu, S. Yin, P.K. Shen, Electrochem. Energy Rev. 2 (2019) 105−127.

[15] J. Mahmood, F. Li, S.M. Jung, M.S. Okyay, I. Ahmad, S.J. Kim, N. Park, H.Y. Jeong, J.B. Baek, Nat. Nanotechnol. 12 (2017) 441–446.

[16] S. Yuan, Z.H. Pu, H. Zhou, J. Yu, I.S. Amiinu, J. W. Zhu, Q.R. Liang, J. L. Yang, D.P. He, Z.Y. Hu, G.V. Tendeloo, S.C. Mu, Nano Energy 59 (2019) 472–480.

[17] Z.H. Pu, I.S. Amiinu, Z.K. Kou, W.Q. Li, S. C. Mu, Angew. Chem. Int. Ed. 56 (2017) 11559–11564.

[18] Z.H. Pu, J.H. Zhao, I.S. Amiinu, W.Q. Li, M. Wang, D.P. He, S.C. Mu, Energy Environ Sci, 2019, 12, 952-957.

[19] Z.H. Pu, S.Y. Wei. Z.B. Chen, S.C. Mu, Appl. Catal. B: Environ. 196 (2016) 193–198.

[20] Y.G. Li, H.L. Wang, L.M. Xie, Y.Y. Liang, G.S. Hong, H.J. Dai, J. Am. Chem. Soc. 133 (2011) 7296–7299.

[21] X.Y. Zhang, J. C. Wang, T. Guo, T.Y. Liu, Z.Z. Wu, L.G. Cavallo, Z. Cao, D.Z. Wang, Appl. Catal. B: Environ. 247 (2019) 78–85.

[22] Q.R. Liang, H.H. Jin, Z. Wang, Y.L. Xiong, S. Yuan, X.C. Zeng, D.P. He, S.C. Mu, Nano Energy, 2019, 57, 746.

[23] J. Xiong, W.W. Cai, W.J. Shi, X.L. Zhang, J. Li, Z.H. Yang, L.G. Feng, H.S. Cheng, J. Mater. Chem. A 5 (2017) 24193−24198.

[24] P. Xiao, W. Chen, X. Wang, Adv. Energy Mater. 5 (2015) 1500985.

[25] X.X. Zou, Y. Zhang, Chem. Soc. Rev. 44 (2015) 5148−5180.

[26] M.A. Khan, H. Zhao, W. Zou, Z. Chen, W. Cao, J. Fang, J. Xu, L. Zhang, J. Zhang, Electrochem. Energy Rev. 1 (2018) 483−530.

[27] J. Deng, H.B. Li, S.H. Wang, D. Ding, M.S. Chen, C. Liu, Z.Q. Tian, K.S. Novoselov, C. Ma, D.H. Deng, X.H. Bao, Nat. Commun. 8 (2017) 14430.

[28] S. Chen, S.Z. Qiao, ACS Nano 7 (2013) 10190−10196.

[29] Q.Q. Sun, Y.J. Dong, Z.L. Wang, S.W. Yin, C. Zhao, Small 14 (2018) 1704137.

[30] B.T. Yonemoto, G. S. Hutchings, F. Jiao, J. Am. Chem. Soc. 136 (2014) 8895−8898.

[31] X.D. Huang, K. Qian, J. Yang, J. Zhang, L. Li, C. Z. Yu, D. Y. Zhao, Adv. Mater. 24 (2012) 4419−4423.

[32] B.G. Choi, M. Yang, W.H. Hong, J.W. Choi, Y.S. Huh, ACS Nano 6 (2012) 4020−4028.

[33] K. Shen, L. Zhang, X. D. Chen, L. M. Liu, D.L. Zhang, Y. Han, J.Y. Chen, J.L. Long, R. Luque, Y.W. Li, B.L. Chen, Science 359 (2018) 206−210.

[34] H. Kim, J. Cho, Chem. Mater. 20 (2008) 1679−1681.

[35] B.Y. Guan, L. Yu, X.W. Lou, Adv. Sci. 4 (2017) 1700247.

[36] Y. Jiang, Y.Z. Lu, J.Y. Lin, X. Wang, Z.X. Shen, Small Methods 2 (2018) 1700369.

[37] J.S. Li, S. Zhang, J.Q. Sha, H. Wang, M.Z. Liu, L. Kong, G.D. Liu, ACS Appl. Mater. Interfaces 10 (2018)17140−17146.

[38] M.A.R. Anjum, J.S. Lee, ACS Catal. 7 (2017) 3030−3038.

[39] Y.Y. Chen, Y. Zhang, W.J. Jiang, X. Zhang, Z. Dai, L.J. Wan, J.S. Hu, ACS Nano 10 (2016) 8851−8860.

[40] J. Deng, P. J. Ren, D. H. Deng, X.H. Bao, Angew. Chem. Int. Ed. 54 (2015) 2100−2104.

[41] J. Zhang, L. Qu, G. Shi, J. Liu, J. Chen, L. Dai, Angew. Chem. Int. Ed. 55 (2016) 2230–2234.

[42] M. Sun, H.J. Liu, J.H. Qu, J.H. Li, Adv. Energy Mater. (2016) 1600087.

[43] X.X. Liu, L. Zhang, M.X. Li, X.L. Hu, Chem. Commun. 54 (2018) 2502−2505.

[44] G. Zhang, G.C. Wang, Y. Liu, H.J. Liu, J.H. Qu, J.H. Li, J. Am. Chem. Soc. 138 (2016) 14686−14693.

[45] Y.M. Shi, B. Zhang, Chem. Soc. Rev. 45 (2016) 1529−1541.

[46] R.G. Ma, Y. Zhou, Y.F. Chen, P.X. Li, Q. Liu, J.C. Wang, Angew. Chem. Int. Ed. 54 (2015) 14723−14727.

[47] F.M. Wang, Y.C. Li, T.A. Shifa, K.L. Liu, F. Wang, Z.X. Wang, P. Xu, Q.S. Wang, J. He, Angew. Chem. Int. Ed. 55 (2016) 6919−6924.

[48] Y. Jia, L.Z. Zhang, G P. Gao, H. Chen, B. Wang, J.Z. Zhou, M.T. Soo, M. Hong, X.C. Yan, G.R. Qian, J. Zou, A.J. Du, X.D. Yao, Adv. Mater. 29 (2017) 1700017.

[49] Z.J. Chen, G.X. Cao, L.Y. Gan, H. Dai, N. Xu, M.J. Zang, H.B. Dai, H. Wu, P. Wang, ACS Catal. 8 (2018) 8866−8872.

[50] R. Borup, J. Meyers, B. Pivovar, Y.S. Kim, R. Mukundan, N. Garland, D. Myers, M. Wilson, F. Garzon, D. Wood, P. Zelenay, K. More, K. Stroh, T. Zawodzinski, J. Boncella, J.E. McGrath, M. Inaba, K. Miyatake, M. Hori, K. Ota, Z. Ogumi, S. Miyata, A. Nishikata, Z. Siroma, Y. Uchimoto, K. Yasuda, K.I. Kimijima, N. Iwashita, Chem. Rev. 107 (2007) 3904−3951.

[51] J.M. Mcenaney, J.C. Crompton, J.F. Callejas, E.J. Popczun, A.J. Biacchi, N.S. Lewis, R.E. Schaak, Chem. Mater. 26 (2014) 4826−4831.

[52] M.Q. Wang, C. Ye, M.W. Xu, S.J. Bao, Nano Res. 11 (2018) 4728–4734.

[53] X.K. Huang, X. Wang, P.B. Jiang, K. Lan, J.H. Qin, L. Gong, K.Z. Wang, M.Yang, L.Ma, R. Li, Inorg. Chem. Front., 2019, 6, 1482–1489.

[54] K. Ojha, M. Sharma, H. Kolev, A. K. Ganguli, Catal. Sci. Technol. 2017, 7, 668–676.

[55] Z.C. Xing, Q. Liu, A.M. Asiri, X. P. Sun, Adv. Mater. 26 (2014) 5702−5707.

[56] Y.F. Zhang, J. Yang, Q.C. Dong, H.B. Geng, Y. Zheng, Y.L. Liu, W.J. Wang, C.C. Li, X.C. Dong, ACS Appl. Mater. Interfaces, 10 (2018) 26258−26263.

[57] J.S. Li, J.Q. Sha, B. Du, B. Tang, Chem. Commun. 53 (2017) 12576−12579.

[58] J.T. Zhang, X.D. Wang, Y.R. Xue, Z.Y. Xu, J.J. Pei, Z.B. Zhuang, Inorg. Chem. 57 (2018) 13859−13865.

[59] J.S. Li, Y. Wang, C.H. Liu, S.L. Li, Y.G. Wang, L.Z. Dong, Z.H. Dai, Y.F. Li, Y.Q. Lan, Nat. Commun. 7 (2016) 11204.

[60] X. Zhang, X.L. Yu, L.J. Zhang, F. Zhou, Y.Y. Liang, R.H. Wang, Adv. Funct. Mater. 28, (2018) 1706523.

[61] Q.R. Liang, H.H. Jin, Z. Wang, Y.L. Xiong, S. Yuan, X.C. Zeng, D.P. He, S.C. Mu, Nano Energy 57 (2019) 746−752.

[62] J. Yang, F.J. Zhang, X. Wang, D.S. He, G. Wu, Q.H. Yang, X. Hong, Y.E. Wu, Y.D. Li, Angew. Chem. Int. Ed. 2016, 551, 2854−12858.

[63] B.C. Liu, H. Li, B. Cao, J.N. Jiang, R. Gao, J. Zhang, Adv. Funct. Mater. 28 (2018) 1801527.

[64] H.J. Yan, Y.Y. Xie, Q. Jiao, A.P. Wu, C.G. Tian, X.M. Zhang, L. Wang, H.G. Fu, Adv. Mater. 30 (2018) 1704156.

[65] J.J. Duan, S. Chen, M. Jaroniec, S.Z. Qiao, ACS Nano 9 (2015) 931−940.

[66] Z.K. Kou, T.T. Wang, Y. Cai, C. Guan, Z.H. Pu, C.R. Zhu, Y.T. Hu, A.M. Elshahawy, J. Wang, S.C. Mu, Small Methods 2 (2018) 1700396.

[67] F. Zhang, T.Y. Liu, M.Y. Li, M.H. Yu, Y. Luo, Y.X. Tong, Y. Li, Nano Lett. 2017, 17, 3097−3104.

[68] S.H. Bae, J.E. Kim, H. Randriamahazaka, S.Y. Moon, J.Y. Park, I.K. Oh, Adv. Energy Mater. 7 (2017) 1601492.

[69] J. Zhao, H.W. Lai, Z.Y. Lyu, Y.F. Jiang, K. Xie, X.Z. Wang, Q. Wu, L.J. Yang, Z. Jin, Y.W. Ma, J. Liu, Z. Hu, Adv. Mater. 27 (2015) 3541−3545.

[70] F. Yu, X.L. Xu, H.G. Peng, H.J. Yu, Y.F. Dai, W.M. Liu, J.W. Ying, Q. Sun, X. Wang, Appl. Catal. A: Gen. 507 (2015) 109−118.

[71] J. Wang, K. Chang , Z. Sun, J.H. Lee, B.M. Tackett, C. Zhang, J.G. Chen, C.J. Liu, Appl. Catal. B:Environ. 251 (2019) 162−167.

[72] M. Sevilla, A.B. Fuertes, ACS Nano 8 (2014) 5069−5078.

[73] M.H. Wei, Y. Luo, C. Jin, J. Sui, Z.J. Wang, C. Li, R.Z. Yang, ACS Appl. Energy Mater. 1 (2018) 331−335.

[74] X.F. Sun, L. Lu, Q.G. Zhu, C.Y. Wu, D.X. Yang, C.J. Chen, B.X. Han, Angew. Chem. Int. Ed. 57 (2018) 2427−2431.

[75] Y.C. Huang, J.X. Ge, J. Hu, J.W. Zhang, J. Hao, Y.G. Wei, Adv. Energy Mater. 8 (2018) 1701601.

[76] L.J. Yang, J.Y. Yu, Z.Q. Wei, G.X. Li, L.D. Cao, W.J. Zhou, S.W. Chen, Nano Energy 41 (2017) 772–779.

[77] F.L. Yang, Y.T. Chen, G.Z. Cheng, S.L. Chen, W. Luo, ACS Catal. 7 (2017) 3824−3831.

[78] Y.P. Zhu, G. Chen, X.M. Xu, G.M. Yang, M.L. Liu, Z.P. Shao, ACS Catal. 7 (2017) 3540−3547.

[79] S. Reddy, R. Du, L.X. Kang, N. Mao, J. Zhang, Appl. Catal. B: Environ. 194 (2016) 16−21.

[80] L.N. Zhang, S.H. Li, H.Q. Tan, S.U. Khan, Y.Y. Ma, H.Y. Zang, Y.H. Wang, Y.G. Li, ACS Appl. Mater. Interfaces 9 (2017) 16270−16279.

[81] H.L. Lin, Z.P. Shi, S.N. He, X.Yu, S.N. Wang, Q.S. Gao, Y. Tang, Chem. Sci. 7 (2016) 3399−3405.

[82] Z.H. Pu, I.S. Amiinu, X.B. Liu, M. Wang, S.C. Mu, Nanoscale 8 (2016) 17256−17261.

[83] C.Y. Tang, W. Wang, A.K. Sun, C.K. Qi, D.Z. Zhang, Z.Z. Wu, D.Z. Wang, ACS Catal. 5 (2015) 6956−6963.